NSRRC-J04333 (2014)

Macromolecules

Article

pubs.acs.org/Macromolecules

Functionalized Nanoporous Gyroid SiO_2 with Double-Stimuli-Responsive Properties as Environment-Selective Delivery Systems

Hui-Chun Lee,[†] Han-Yu Hsueh,[†] U-Ser Jeng,[†,‡] and Rong-Ming Ho*[,†]

[†]Department of Chemical Engineering, National Tsing Hua University, Hsinchu 30013, Taiwan

[‡]National Synchrotron Radiation Research Center, 101 Hsin-Ann Road, Hsinchu Science Park, Taiwan

Supporting Information

ABSTRACT: Herein, we aim to fabricate nanoporous gyroid SiO_2 from templated sol–gel reaction using degradable block copolymer with gyroid-forming nanostructure as a template and then to functionalize the nanoporous materials using "smart" polymer, poly(2-(dimethylamino)ethyl methacrylate) (PDMAEMA), brushes via the "grafting from" method to give double-stimuli-responsive properties. By taking advantage of the responses to environmental stimuli, both thermal and pH, the pore features can be well-defined by the stretching and recoiling of PDMAEMA brushes because of their adjustable chain conformations with reversible character. The responsive properties with respect to environmental stimuli can be successfully traced by temperature-resolved small-angle X-ray scattering (SAXS) in aqueous environment. Owing to the high specific surface area and porosity, 3D pore network, biocompatibility, and environmental responses, the functionalized nanoporous gyroid SiO_2 is further demonstrated as a stimuli-responsive controlled release system.

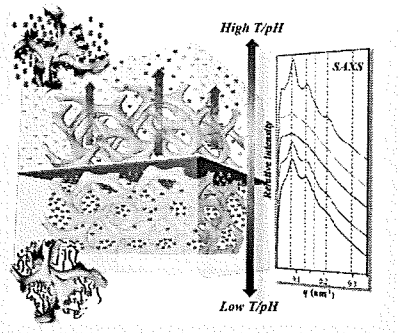

INTRODUCTION

A biomimetic interface with adjustable chemical and/or physical properties that can adapt to surrounding environments is essential in many applications, and how to achieve materials with interfacial functions becomes a chief mission in diverse areas. Accordingly, smart materials involving porous templates and stimuli-responsive gates capable of reversible switching or adjusting their permeation behaviors in response to environmental stimuli have long been an important subject due to the great potential in applications, such as molecular separation, water filtration, medical engineering, environmental sensing, and controlled release.[1,2] Porous materials with versatile characters contributed by individual composition, morphology, and functionality gradually become predominant in materials research due to their distinctive material features, such as well-defined pore texture and mechanical property.[3−5] For instance, anodized aluminum oxide (AAO) films with cylinder pores[6] have been widely exploited in various fields and already commercially available. In contrast to the low biocompatibility of the AAO, mesoporous silica (i.e., MCM materials)[7] characterized by high specific surface area,[8] environmental resistance, nontoxic nature, and easy postfunctionalization has been developed to boost applications using porous materials. Recently, block copolymers (BCPs) have been extensively investigated because of their abilities to self-assemble as various ordered nanostructures with nanoscale size ranging from 10 to 50 nm.[9,10] Moreover, the feasibility to acquire large-area continuous monoliths from self-assembly makes them appealing for applications in nanotechnologies.[11] By taking advantage of the degradable character of constituted components in the BCPs, nanoporous materials can be facilely prepared by selectively removing the degradable block through hydrolysis, ozonization, reactive ion etching, or UV.[12−19] Among all of the nanostructures formed by the self-assembly of BCPs, double gyroid (DG) is one of the most appealing morphologies for practical applications because of its unique geometry, comprising a matrix and two cocontinuous but independent, interpenetrating networks (i.e., single gyroid (SG)) in three-dimensional space.[20−22] As a result, it is possible to create nanoporous materials with well-ordered texture and open-cell character by degradation of the networks so that its higher specific surface area and porosity than other regular nanostructured phases[23] give rise to outstanding properties including fast transport and/or exchange of substances, isotropic percolation not necessary for structure alignment before utilization, and 3D pores without dead ends for applications.[24−30] Note that it is necessary to provide well-controlled orientation for a hexagonal morphology with open-cell character. Also, for a lamellar morphology, it is difficult to create a free-standing porous texture.

In addition to the physical properties of the nanoporous materials, the functionalities of the material framework and pore surface are critical in practical applications, such as nanoreactor,[31−35] filter,[24,36−39] sensor,[40,41] biomimetic gate,[42−45] and especially controlled release system.[46−50] Over the past decade, a lot of attention has been given to stimuli-responsive polymers, also termed "smart materials", that respond to environmental stimuli, for example, pH, temper-

Received: February 17, 2014
Revised: April 8, 2014
Published: April 18, 2014

 © 2014 American Chemical Society

Scheme 1. Schematic Illustration for the Fabrication of PDMAEMA-Functionalized Nanoporous Gyroid SiO_2

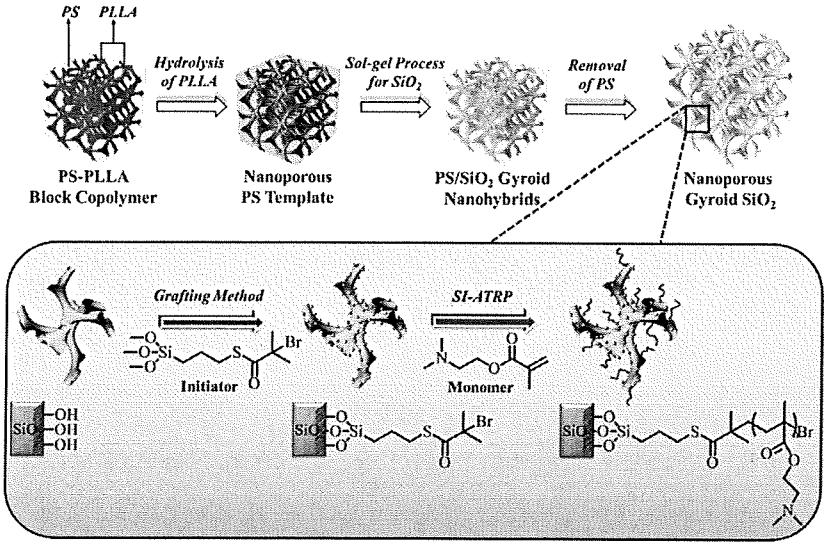

ature, light, ultrasound, and so on.[2,42,44,45,51−57] Poly(2-(dimethylamino)ethyl methacrylate) (PDMAEMA) has attracted increasing interest for its unique features of buffering capacity and less cytotoxicity.[58−61] Most interestingly, the environmental response of the PDMAEMA is strongly dependent upon its lower critical solution temperature (LCST) and the corresponding pH value in aqueous solution.[61−64] As a result, the PDMAEMA is referred as a polymer with double-stimuli response. Müller and co-workers reported the double-stimuli-responsive porous membrane with controlled water flux by using self-supporting polystyrene-*b*-PDMAEMA BCPs.[61] As demonstrated in the report, the pore size is a function of temperature and also the environmental pH value of the membrane in water so that the membrane can be used as the device for particle size selectivity. Nevertheless, it is still a challenge to find facile methods for fabrication of biocompatible, high environmental resistance, and highly efficient materials with double responsive properties.

Herein, we suggest a simple method for fabrication of a PDMAEMA-functionalized nanoporous gyroid SiO_2, equipped with well-defined structure, efficient porous texture, environmentally resistance, and biocompatibility. By taking advantage of the responses of the PDMAEMA to environmental stimuli, the pore features can be well-defined by stretching and recoiling of the PDMAEMA brushes because of their adjustable chain conformations in response to temperature and/or pH. Owing to the high porosity of the network morphology and the biocompatibility of SiO_2, the functionalized nanoporous gyroid SiO_2 can be applied to accomplish the environment-selective delivery pattern, which can further improve the therapeutic efficiency and specificity. Scheme 1 illustrates the general process to fabricate the PDMAEMA-functionalized nanoporous gyroid SiO_2. Polystyrene-*b*-poly(L-lactide) (PS−PLLA) BCPs with gyroid morphology were prepared according to the procedures previously reported.[65] The PLLA framework is first selectively removed by hydrolysis, giving nanoporous PS template for sol−gel process. The gyroid-forming nanochannel is then replaced by SiO_2 through templated sol−gel reaction of tetraethyl orthosilicate (TEOS). Subsequently, calcination is utilized to remove the PS matrix, giving nanoporous gyroid SiO_2 with well-defined gyroid structure and high porosity.[66] The postfunctionalization of the nanoporous gyroid SiO_2 with PDMAEMA brushes is applied to convert SiO_2 to biomimetic "smart" materials. Our strategy starts from the grafting of halogen-functionalized initiator, 2-bromothioisobutyrate (MPTS-Br),[67] by utilizing the hydroxy groups on the interface. Subsequently, surface-initiated atom transfer radical polymerization (SI-ATRP) is carried out to graft the double-stimuli-responsive polymer, PDMAEMA, from the SiO_2 surface.[68]

EXPERIMENTAL SECTION

Materials. All the reagents, catalysts, and solvents were used as received unless otherwise noted. Styrene was filtered through a column half-filled with silica gel, and L-lactide was purified by recrystallization from toluene.[65]

Synthesis of Nanoporous Gyroid SiO_2. The PS−PLLA with gyroid texture utilizing in this study was synthesized by a two-step process, and the details of characterization were described in our previously published results (see ref 65). The number-average molecular weight (M_n) and the molecular-weight dispersity (M_n/M_w, $Đ_M$) of the PS component were first determined by GPC. The $Đ_M$ of PS−PLLA was determined by GPC and the repeating numbers of L-LA versus styrene were then determined by ^{1}H NMR. The M_n of the PS and the PLLA and the $Đ_M$ of the synthesized PS−PLLA are 37 600 g/mol, 25 200 g/mol, and 1.32, respectively. The volume fraction of PLLA constituent, f_{PLLA}^v, is calculated as 0.35 by assuming that the densities of PS is 1.02 g/cm^3 and the PLLA is 1.25 g/cm^3. The lattice constant of the PS−PLLA was determined by SAXS as approximately 124 nm. Then, the general processes to fabricate nanoporous SiO_2 with the gyroid morphology from the original PS−PLLA template is demonstrated in our previous work.[66]

Synthesis of Halogen-Functionalized Initiator (MPTS-Br). The α-bromoisobutyryl bromide (25.75 mmol) was added dropwise to the stirred solution of 3-(mercaptopropyl)trimethoxysilane (25.6 mmol) and triethylamine (25.6 mmol) in dry toluene (42.5 mL) under a nitrogen atmosphere with cooling in an ice bath, and the solution was then stirred overnight at room temperature. The product was distilled under reduced pressure to give the ATRP initiator 2-bromothioisobutyrate;[67] 500 MHz ^{1}H NMR in $CDCl_3$ was used to characterize (Figure S1, Supporting Information).

ATRP of PDMAEMA. Modification from the literature,[68] the ATRP procedure to prepare PDMAEMA was typical as follows: DMAEMA (2.33 g, 14.8 mmol), CuBr (0.059 g, 0.41 mmol), HMTETA (0.07 g,

dx.doi.org/10.1021/ma500360a | Macromolecules 2014, 47, 3041−3051

0.30 mmol), and DHI_4-Br (0.06 g, 0.25 mmol) were introduced into a 100 mL Schlenk flask with a magnetic stirrer at 65 °C for 24 h. The synthesis was characterized by ^1H NMR (500 MHz in $CDCl_3$ at 298 K, ^2H, $-CH_2-$, δ = 4), and the molecular weight (M_n) and the molecular-weight dispersity (M_n/M_w, $Đ_M$) were determined by GPC.

Synthesis of PDMAEMA-Functionalized Nanoporous Gyroid SiO_2. The nanoporous gyroid SiO_2 (10 mg) was immersed into a solution of the MPTS-Br (5 wt %) in toluene (10 mL), and the mixture was gently refluxed for 6 h. The MPTS-Br functionalized nanoporous gyroid SiO_2 was washed by ultrasonic bath in fresh toluene for 3 min and dried under vacuum at 80 °C. After the initiator functionalized nanoporous gyroid SiO_2 was fabricated, SI-ATRP was carried out to graft PDMAEMA from the SiO_2 surface.

Synthesis of Riboflavin-Loaded PDMAEMA-Functionalized Nanoporous Gyroid SiO_2. Riboflavin was dissolved in dimethyl sulfoxide (DMSO) at a concentration of 40 mg mL^{-1}. PDMAEMA functionalized nanoporous gyroid SiO_2 (10 mg) was added to the solution (5 mL), and then the mixture was shaken for 3 days at room temperature to reach the equilibrium under dark environment. The template was washed with the PBS buffer at pH 1.5 for three times and dried under vacuum.

Characterization. All ^1H nuclear magnetic resonance spectroscopy (NMR) were recorded on a Varian Unity INOVA 500 NMR spectrometer in *d*-chloroform at a concentration of 1 wt %. Small-angle X-ray Scattering (SAXS) experiments were conducted at the synchrotron X-ray beamline 23A with a Pilatus 1M hybrid pixel detector (Dectris) at NSRRC, Hsinchu. All the spectra of Fourier transform infrared spectroscopy (FTIR) were collected on a PerkinElmer SYSTEM-2000 spectrometer at a resolution of 1 cm^{-1}. Thermal stability of samples was measured by PerkinElmer Pyrisl thermogravimetric analysis (TGA) with a heating rate of 10 °C/min from room temperature to 700 °C under a N_2 atmosphere. The observations of field-emission scanning electron microscopy (FESEM) were performed on a JEOL JSM-6700F using accelerating voltages of 1.5–3 keV. Bright-field transmission images of transmission electron microscopy (TEM) were performed on a JEM-2100 (HT) (LaB_6) using an accelerating voltage of 200 kV. For the environment-selective delivery study, the releasing medium (3 mL) was removed at given time interval and diluted to a proper concentration. The fluorescence spectroscope (Hitachi FL-2500) was utilized, and the PL spectra were obtained at a excitation wavelength of 286 nm with a scan speed of 300 nm/min.

RESULTS AND DISCUSSION

Fabrication of Nanoporous Gyroid SiO_2. Figure 1a shows the TEM projection of the gyroid-forming PS–PLLA with RuO_4 staining at which the PS matrix appears dark and the bright frameworks are PLLA. The [110] projection image and corresponding one-dimensional SAXS (1D SAXS) results with reflections found at the relative q values of $\sqrt{6}:\sqrt{8}:\sqrt{14}:\sqrt{16}:\sqrt{32}:\sqrt{50}$ (Figure 1d) suggest the formation of the gyroid phase. After hydrolysis to remove the PLLA frameworks, nanoporous PS template can be fabricated and used as a template for sol–gel reaction to form the PS/SiO_2 gyroid nanohybrids. Figure 1b presents the [110] projection of the PS/SiO_2 gyroid nanohybrids without staining; the reversed mass–thickness contrast compared to Figure 1a demonstrates that the PLLA microdomains are well substituted by SiO_2. Figures 1e and 1f show the corresponding 1D SAXS for the nanoporous PS and the PS/SiO_2, respectively. For nanoporous PS template, the relative q values are similar to the intrinsic PS–PLLA at which the relative q values of $\sqrt{6}:\sqrt{8}:\sqrt{14}:\sqrt{16}:\sqrt{32}:\sqrt{50}$ can be found, indicating successful removal of the PLLA blocks. For the PS/SiO_2 nanohybrids, the formation of well-defined gyroid phase can be evidenced by the reflections at the relative q values of $\sqrt{4}:\sqrt{6}:\sqrt{8}:\sqrt{20}$. Note that the appearance of small $\sqrt{4}$

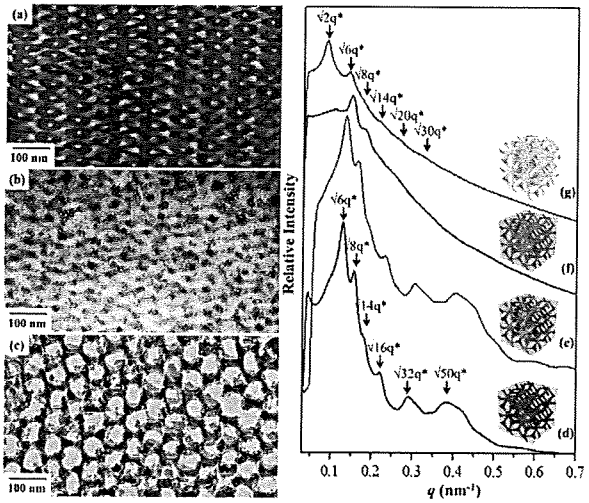

Figure 1. TEM images of (a) gyroid-forming PS–PLLA with RuO_4 staining, (b) PS/SiO_2 gyroid nanohybrids without staining, and (c) nanoporous gyroid SiO_2 without staining. Corresponding one-dimensional SAXS profiles of (d) PS–PLLA, (e) porous PS, (f) PS/SiO_2, and (g) nanoporous gyroid SiO_2.

reflection should be attributed to the deformation of gyroid structure during the templated sol–gel reaction.[69,70] Also, an obvious shift to the high q for the characteristic primary peaks at a q ratio of $\sqrt{6}$ and $\sqrt{8}$ (Figure 1f) can be clearly identified, reflecting a significant shrinkage of the interdomain spacing of the gyroid phase after sol–gel process. The reduction in the interdomain spacing is attributed to the swelling of the PS matrix by methanol followed by the formation of SiO_2 dry gel, resulting in a decrease in proportional dimension of the texture during the aging process. After removal of the PS matrix by calcination, nanoporous gyroid SiO_2 with well-defined nanoporous texture can be formed, as evidenced by TEM image (Figure 1c). The preservation of gyroid nanostructure from the PS/SiO_2 nanohybrids to nanoporous SiO_2 can be further evidenced by 1D SAXS with the relative q values of $\sqrt{2}:\sqrt{6}:\sqrt{8}:\sqrt{14}:\sqrt{20}:\sqrt{32}$ (Figure 1g). In contrast to the scattering results from the PS/SiO_2 gyroid nanohybrids, the $\sqrt{2}$ peak can be clearly identified in addition to extra diffractions in high q region, but the expected (110) reflection (i.e., $\sqrt{4}$ peak) is missing. As described in previous study,[66] the appearance of the $\sqrt{2}$ reflection is attributed to the phase transition of the SiO_2 networks (i.e., the formation of anisotropic gyroid nanostructure) during calcination for the removal of PS matrix. The bicontinuous inorganic networks are still reorganized after removal of the PS matrix, but the loss of registration between the two frameworks contributes a new SAXS reflection, which can be indexed as the $I4_132$, single gyroid-like (SG-like) structure. Obviously, the shifting in the intrinsic gyroid grain should be a random event and would break the symmetry of the original structure, double gyroid (DG), forming a structure without central symmetry, in other words, the formation of two separated networks as SG. Accordingly, through the random shifting, the outcome morphology in the self-assembled sample will transform from a intrinsic DG nanostructure with a space group of $Ia\bar{3}d$ to a SG-like nanostructure with a space group of $I4_132$.[71,72] On the basis of the Brunauer, Emmett, and Teller (BET) method (Figure S2, Supporting Information), the specific surface area

dx.doi.org/10.1021/ma500360a | Macromolecules 2014, 47, 3041–3051

and the porosity of the nanoporous gyroid SiO_2 were calculated as 980 m^2/g and 62%, respectively. By comparing our results with the results from gyroid MCM-48 systems,[8] the MCM-48 systems equipped with the specific surface area values from 660 to 1010 m^2/g and with the porosity from 54% to 64% can be obtained; hence, the fabricated nanoporous gyroid SiO_2 in this study is very competitive by possessing extremely high porosity and specific surface area.

Characterization of PDMAEMA-Functionalized Nanoporous Gyroid SiO_2. Functionalization of nanoporous gyroid SiO_2 by double-stimuli-responsive polymer, PDMAEMA, was carried out by surface-initiated atom transfer radical polymerization (SI-ATRP) using the MPST-Br as grafting initiator. The corresponding chemical reactions from PS–PLLA to nanoporous gyroid SiO_2 are characterized by FTIR. Starting from PS–PLLA, the absorption at 1750 cm^{-1} in the FTIR spectrum is attributed to the C=O of PLLA whereas the absorptions at around 690 and 3050–3100 cm^{-1} are attributed to the C=C of PS, and the corresponding benzene absorption is at 1600 cm^{-1} (Figure 2a). After hydrolysis, signal standing for PLLA

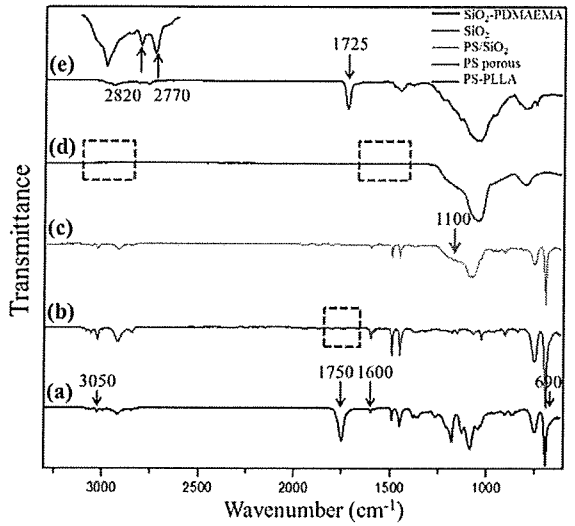

Figure 2. FTIR spectra of (a) PS–PLLA BCPs, (b) gyroid-forming PS templates, (c) PS/SiO_2 nanohybrids, (d) nanoporous gyroid SiO_2, and (e) PDMAEMA-functionalized nanoporous gyroid SiO_2.

disappears due to the hydrolysis of the PLLA (Figure 2b). Subsequently, the broaden peak at around 1100 cm^{-1} that represents Si–O of SiO_2 can be found in PS/SiO_2 nanohybrids, reflecting the formation of SiO_2 from templated sol–gel reaction (Figure 2c). After calcination for the remove of PS matrix, nearly all the polymer related signals vanish, indicating the successful fabrication of nanoporous gyroid SiO_2 (Figure 2d). As shown in Figure 2e, the appearance of characteristic absorptions at around 2700–2800 and 1725 cm^{-1} standing for $-CH_2-$ near the nitrogen atom and C=O evidence the grafting of PDMAEMA on the nanoporous gyroid SiO_2.

TGA measurements, was used to examine the relative composition of grafted PDMAEMA brushes within the functionalized nanoporous SiO_2. As shown in Figure S3, the first step for the weight loss at a mass loss of 7.5% is related to the degeneration of the initiator, and the second step for the weight loss at a mass loss of 31% starting from 200 °C is attributed to the decomposition of the PDMAEMA, suggesting that there is approximately 25% of the grafted PDMAEMA in the nanoporous gyroid SiO_2. The nanoporous gyroid SiO_2 is stable even at 700 °C because of its outstanding thermal stability. To further examine the effect of initiator concentration on the grafting density of PDMAEMA, different concentrations of the initiator were used for the grafting reaction (see Supporting Information for details). As found in the grafted SiO_2, a significant increase in the grafting density can be achieved by using higher initiator concentration (say 5 wt % in comparison to 0.2 wt %), as evidenced by the weight loss of 3% in the toluene solution with 0.2 wt % initiator (Figure S3b) but the increasing loss of 7.5% in 5 wt % treatment (Figure S3c). Accordingly, the TGA measurements indicate that the amount of the grafted PDMAEMA might be able to be controlled by the use of the initiator concentration.

To further investigate the functionalized nanoporous gyroid SiO_2, the nanoporous samples were examined by microscopic observations. Before functionalization, as shown in Figure 3a,

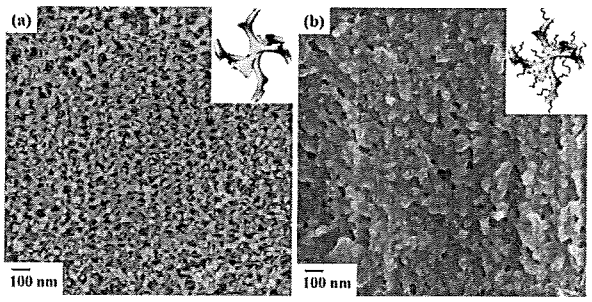

Figure 3. FESEM images of (a) nanoporous gyroid SiO_2 and (b) PDMAEMA-fuctionalized nanoporous gyroid SiO_2.

porous texture can be clearly identified in the nanoporous gyroid SiO_2, and the FESEM results are in line with the TEM observations (Figure 1c). By contrast, the population of porous texture will be greatly diminished after functionalization (Figure 3b), indicating that the grafting of PDMAEMA brushes will shield the nanopores. TEM results seem consistently, in contrast to Figure 1c, the dark SiO_2 framework can be shelled with bright regions before RuO_4 staining, indicating the successful grafting of PDMAEMA (Figures 4a and 4b). After RuO_4 staining, the grafted PDMAEMA can be specifically stained, giving significant contrast from SiO_2. Consequently, in contrast to Figures 4a and 4b, inverse mass–thickness contrast with dark PDMAEMA on the periphery of gray SiO_2 framework can be found (Figures 4c and 4d). On the basis of the morphological observations, the functionalization of nanoporous gyroid SiO_2 by PDMAEMA can be further evidenced.

Double-Stimuli-Responsive Properties. To examine the morphological variation of the PDMAEMA-functionalized nanoporous gyroid SiO_2 driven by the applied stimuli, temperature-resolved SAXS experiments in aqueous solution were carried out at different pH environments. It is well-known that the environmental response of the PDMAEMA is a typical LCST behavior; the variation on the PDMAEMA chain conformation is strongly dependent upon temperature and the corresponding pH value in aqueous solution; for example, the LCST at pH 2 is above 85 °C, at pH 7 is around 65 °C, and is below 35 °C once the pH raises to 11.[61,63,64] Accordingly, to demonstrate the corresponding conformational changes of the

dx.doi.org/10.1021/ma500360a | Macromolecules 2014, 47, 3041–3051

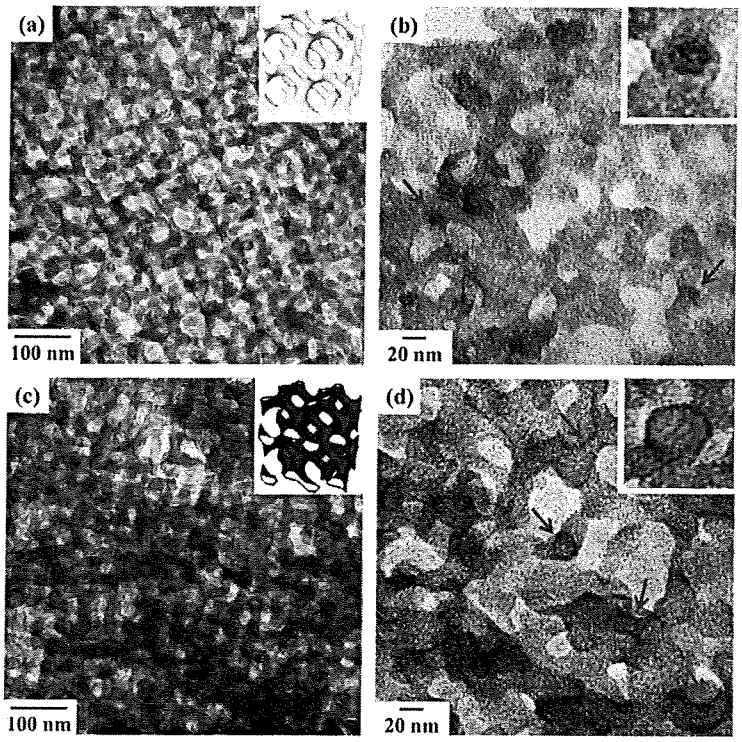

Figure 4. TEM images of (a) PDMAEMA-functionalized nanoporous gyroid SiO_2 w/o RuO_4 staining; (b) enlarged image of (a). The inset shows the dark SiO_2 framework shelled with gray PDMAEMA. (c) PDMAEMA-functionalized nanoporous gyroid SiO_2 with RuO_4 staining and (d) enlarged image of (c). The inset shows the inverse contrast with gray SiO_2 framework shelled with dark RuO_4-stained PDMAEMA at which a clear dark line around the periphery can be found.

grafted brushes, environmental conditions were controlled by using solutions with different pH values thermostated at different temperatures. Since the pK_a of the PDMAEMA is approximately 7.4,[61,62] the responses of the polymer conformation are examined with pH values below, near and above 7 (i.e., pH 2, pH 7, and pH 11). Figures 5a to 5c summarize the SAXS data collected for the samples at specific pH environment but various temperatures. Thermal treatment with step-increased temperature from 35 to 75 °C, in an incremental of 10 °C, was applied to trace the morphological evolution of the PDMAEMA-functionalized nanoporous gyroid SiO_2 at individual pH value. Note that, to reach the thermal equilibrium of isothermal treatment, the retention period at the setting temperature was 15 min.

At pH 2, as shown in Figure 5a, all of the 1D SAXS profiles at different temperatures are similar; reflections occur at the relative q values of $\sqrt{2}:\sqrt{6}:\sqrt{8}:\sqrt{14}$. The insensitive results in response to temperature is attributed to the high LCST (>85 °C) at pH 2, resulting from the highly protonated PDMAEMA at acidic environment. Namely, the polymer chains are highly soluble in water and remain as extended conformations even with the increase of temperature. Only at the highest temperature (75 °C) examined, the SAXS reflections will be slightly broadened due to the temperature coming close to the transition temperature. Figure 6 provides a schematic illustration of the proposed mechanism with respect to the scattering length density (SLD) distribution and corresponding conformational transformations of the grafted PDMAEMA at different environments. As shown in Figure 6a, at this situation, the totally extended polymer brushes into the solution filled within the SiO_2 pores contribute to a relatively uniform SLD layer. Note that in these models the calculated SLD values for the SiO_2 frameworks, neat PDMAEMA, Br terminal, and water are 20.6, 10.4, 22.6, and 9.4 in units of 10^{-6} Å^{-2}, respectively. For the protonized PDMAEMA in aqueous solution, the SLD value is estimated to be an average of the uniformly distributed PDMAEMA brushes with Br terminal in H_2O so that the value is obviously higher than water.

By contrast, significant change in the SAXS results can be seen once the pH value reaches 7 (Figure 5b). When the temperature is low (e.g., 35 °C), the scattering results with the reflections at the relative q values of $\sqrt{2}:\sqrt{6}:\sqrt{8}:\sqrt{14}$ can be observed, and similar results can also be found at temperatures lower than the LCST (e.g., 45 °C). Similar to the illustration in Figure 6a, when sample temperature is below the transitional temperature, the fully extended polymer brushes contribute a uniform chain distribution in water within the pores, giving the electron density contrast as illustrated. Interestingly, once the temperature comes close to the LCST (e.g., 55 and 65 °C), the SAXS peaks deteriorate indistinctly, and only the $\sqrt{2}$ and $\sqrt{6}$ reflections can survive barely. Presumably, when close to the LCST transition, polymer chains may be partially extended with unevenly distributed Br terminal within the pores, leading to parabolic-like SLD profiles with dramatic diffusion of the scattering contrast, extending out from grafted SiO_2 walls as shown in Figure 6b, namely, resulting in the unrecognized (i.e., smearing) SAXS reflections; the minimum SLD for the center zone depleted with polymer chains is largely contributed by water of a lowest SLD (9.4×10^{-6} Å^{-2}) compared to the polymer and SiO_2.

dx.doi.org/10.1021/ma500360a | *Macromolecules* 2014, 47, 3041−3051

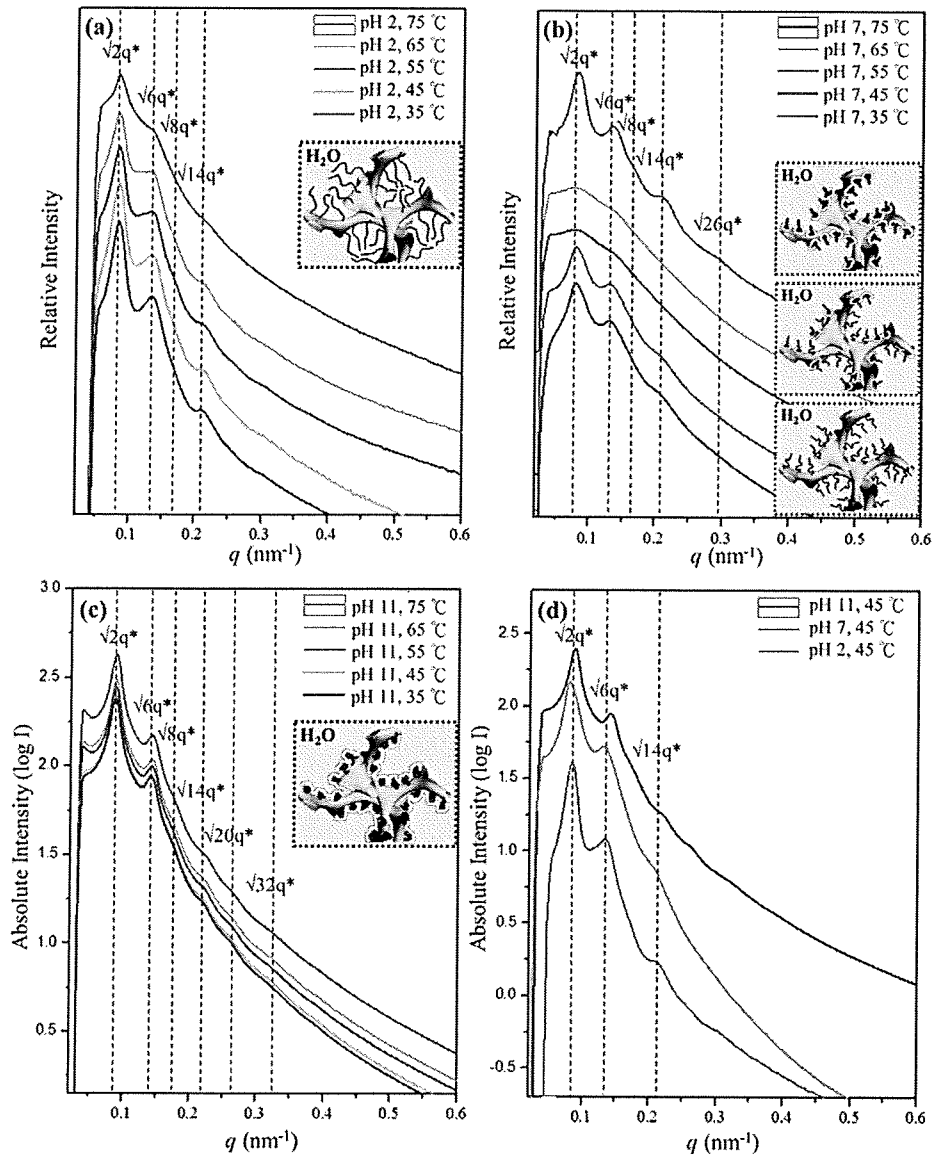

Figure 5. Temperature-resolved SAXS profiles of PDMAEMA-functionalized nanoporous gyroid SiO_2 in solution state with temperature increment from 35, 45, 55, 65 to 75 °C: (a) in acidic environment with pH = 2; (b) in neutral environment with pH = 7; (c) in basic environment with pH = 11. (d) The scattering profiles of PDMAEMA-functionalized nanoporous gyroid SiO_2 in pH 2, pH 7, and pH 11 at 45 °C. Note that the intensity is represented by relative value in (a) and (b) and absolute value in (c) and (d).

Upon the temperature rises above the LCST (e.g., 75 °C), the missing SAXS reflections reappear and become even stronger than the ones at lower temperatures; the reflections with the relative q values of $\sqrt{2}:\sqrt{6}:\sqrt{8}:\sqrt{14}:\sqrt{32}$ can be clearly identified. The enhanced scattering and the occurrence of additional reflections are likely attributed to a sharpened scattering contrast due to the LCST-induced highly retracted polymer chains for better defined polymer–water interfaces (as illustrated in Figure 6c at which the polymer chains become insoluble in water and remain as condensed conformations on the wall of the pore). Because of the uncharged property of PDMAEMA chains in basic situation, the LCST at pH 11 (approximately 35 °C) is lower than all the applied temperatures. Consequently, the polymer chains are expected to largely contract to the SiO_2 walls (Figure 6c) for the prominent SAXS peaks at the relative q values $\sqrt{2}:\sqrt{6}:\sqrt{8}:\sqrt{14}:\sqrt{20}:\sqrt{32}$. Correspondingly, there are no obvious SAXS profile changes over the temperature ranging from 35 to 75 °C studied, and only a gradual increment on reflection intensity with respect to the increase of temperature can be observed (as shown in Figure 5c with the absolute intensity profile). The observed increase in the reflection intensity is attributed to the further condensation of the uncharged PDMAEMA brushes due to the increasing of temperature at base environment. As illustrated in Figure 6c, without the contribution of polymer brushes and Br terminal, a decrease in SLD will give the best scattering contrast from the SiO_2 frameworks (20.6×10^{-6} Å^{-2}) and the space-filled water

dx.doi.org/10.1021/ma500360a | Macromolecules 2014, 47, 3041−3051

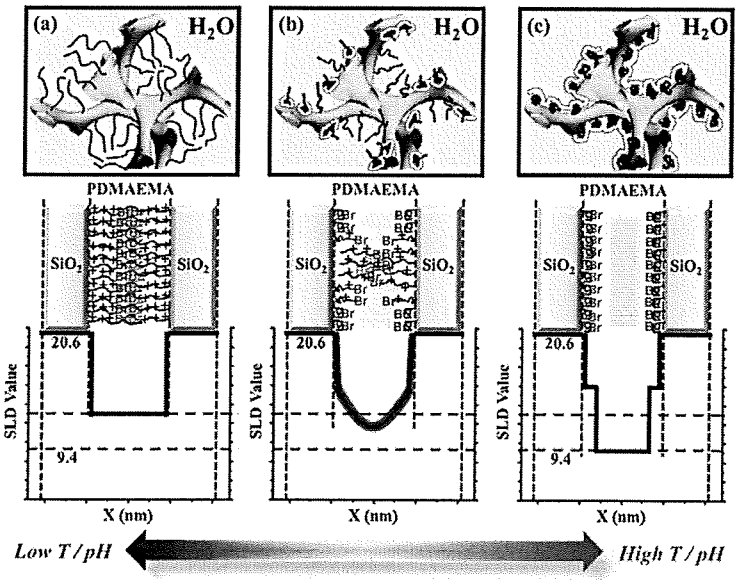

Figure 6. Schematic illustration of suggested conformational transformations of the grafted PDMAEMA brushes on nanoporous gyroid SiO_2 with the corresponding electron density distribution: (a) at low temperature and/or acidic environment; (b) at temperature near the LCST and/or pH around the pK_a (transitional stage); and (c) at high temperature and/or basic environment. The SLD values were calculated by using the scattering length density calculator from National Institute of Standard Technology Center for Neutron Research (see Figure S4, Supporting Information, for details).

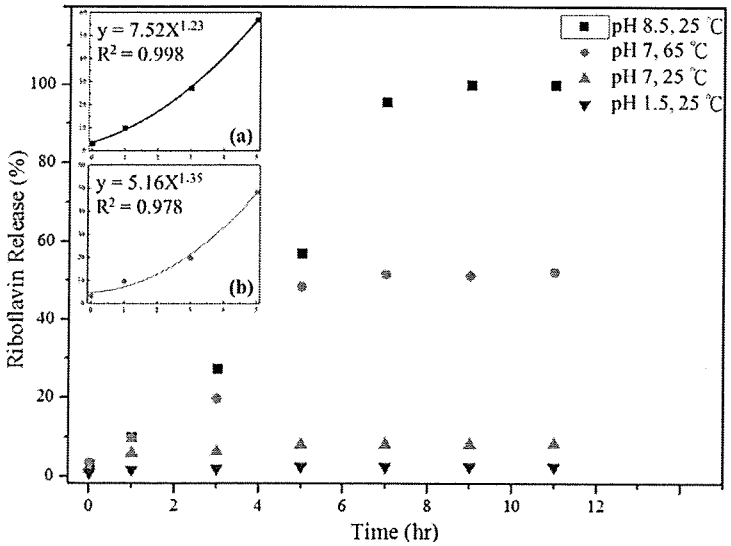

Figure 7. Cumulative release profiles of PDMAEMA-functionalized nanoporous gyroid SiO_2 in response to pH and temperature changes in PBS. Inset (a) plots the fitted curve (blue line) for the release profile at pH 8.5 and 25 °C, and inset (b) plots the fitted curve (orange line) for the release profile at pH 7 and 65 °C.

(9.4×10^{-6} Å^{-2}) so that sharpest scattering peaks is achieved with the fully contracted copolymers grafted on the SiO_2 walls at the highest pH value and temperature used. Figure 5d gives an overview on the sample at constant temperature but various pH environments at which significant change in scattering intensity can be seen from the SAXS profile. At pH 11, the scattering intensity is the highest. It is attributed to the effect of total deprotonization, resulting in the recoil of the examined PDMAEMA brushes; consequently, this provides the sharpest scattering contrast with clear-cut polymer–water interfaces (Figure 6c). Whereas at pH 2, the equally sharp SAXS profile with a lower scattering intensity observed can be attributed to a high protonization of the grafted PDMAEMA brushes, resulting in hydrophilic and fully extended PDMAEMA chain conformation; as illustrated in Figure 6a, the well-mixed polymer–water zones, giving a uniform SLD, provide sharp interfaces but a lower scattering contrast with the SiO_2 walls, compared to that shown in Figure 6c. At pH 7, the pH coming close to the pK_a, less extended PDMAEMA chains due to the reduction in protonization lead to the enhancement of electron density

dx.doi.org/10.1021/ma500360a | *Macromolecules* 2014, 47, 3041–3051

contrast, but with the smeared interfaces. Correspondingly, smearing in the SAXS profiles are observed, especially in high-q region (Figure 5d), indicating the formation of diffused interface as proposed. This smearing effect can be consistently observed whenever the applied temperature comes across the LCST because of the unevenly condensation induced by the LCST effect, resulting in a rough (or fluctuating) SLD transition layer between the SiO_2 walls, giving reduced contrast and diminished SAXS peaks (Figure 6b).

Anomalous small-angle X-ray scattering (ASAXS) was also adapted to examine the SLD schematic proposed in Figure 6. By performing energy-dependent SAXS experiments with the characteristic absorption edge of Br element, energies from E1 (13.4348 keV), E2 (13.4648 keV), to E3 (13.4681 keV) were selected to vary the contrast for scattering of the Br element. At pH = 2 with a fully stretched chain conformation, the concentrated terminal Br groups of the polymer near the center zones of gyroid pore–water regions would contribute to specific ASAXS effects. Indeed, as shown in Figure S5, SAXS peak intensity measured with an X-ray energy (E3, 13.4681 keV) near the resonant X-ray at Br K-edge absorption at 13.474 keV is decreased by 4%, compared to that measured with off-resonant X-rays at 13.4348 keV (E1). The ASAXS result implies that the Br groups on the scattering results can be effective. As a result, we speculate that the parabolic-like SLD profiles (Figure 6b) with dramatic diffusion of the scattering contrast is attributed to the contribution of the SLD of the Br groups, resulting from unevenly distributed Br terminal within the pores. In contrast to the ASAXS results at pH 2, no significant variation can be found at pH 7 while the temperature is close to the LCST.

Environment-Selective Delivery Systems. According to the SAXS and ASAXS results, the responsive properties with respect to both pH and thermal stimuli can be successfully traced in different aqueous environments. Owing to the dynamic responses with respect to pH and temperature, the PDMAEMA-functionalized nanoporous gyroid SiO_2 can be further designed as "smart" nanotechnologies with adjustable properties in response to the environmental variations. To exploit the double-stimuli-responsive properties as controlled release systems, riboflavin (vitamin B_2), an important bioactive molecule involved in various biochemical processes and commonly used as therapeutic drug for vitamin deficiencies, was selected as a model substance to examine the loading and controlled release behaviors of the PDMAEMA-functionalized nanoporous gyroid SiO_2. By taking advantage of splendid photoluminescent (PL) property from riboflavin, the cumulative release profile can be promptly detected by fast fluorescence analysis. Figure 7 shows the cumulative release profiles of riboflavin from riboflavin-loaded PDMAEMA-functionalized nanoporous gyroid SiO_2 in the phosphate buffered saline (PBS) buffer in response to pH change from pH 1.5 (a simulated gastric medium) to pH 8.5 (a simulated intestinal medium) at 25 °C and temperature change from 25 to 65 °C at pH 7.

At pH 1.5 and 25 °C, the release rate of the PDMAEMA-functionalized nanoporous gyroid SiO_2 is extremely slow, and the released amount is trivial even with a long period of 11 h. In contrast, upon the pH value of the releasing medium switching to 8.5 at the same temperature, the system exhibits a release profile with the release amount of 60% within 5 h and also sustained-release property without burst effect until 11 h (Figure S6, Supporting Information, for apparent variation in color). By contrast, at pH 7 and 25 °C (the LCST is around 65 °C), slow release rate with only a slightly higher releasing amount than that at pH 1.5 can be detected. Once the temperature increases to 65 °C (close to the LCST), the system exhibits a sustained-release profile with the released amount around 60% within 5 h. Note that the cumulative release amount at pH 7 and 65 °C is lower than that at pH 8.5 and 25 °C although both conditions give similar release profile. We speculate that the lower cumulative release amount at pH 7 and 65 °C than that at pH 8.5 and 25 °C might be attributed the protonization and less condensed PDMAEMA brushes at pH below pK_a even at high temperature.

On the basis of the suggested model, the significant variations in the release behavior are mainly attributed to the conformational variations (i.e., the double-stimuli-responsive properties) of the grafted PDMAEMA brushes at different environments. Because of the full protonization in acidic environment, the extended PDMAEMA brushes can act as multi blockades that inhibit the openings of the gyroid forming nanochannels while the pH value is below pK_a (pH 7.4)[61,63] and/or the temperature is below the LCST. As a result, at pH 1.5 and 25 °C, the release system gives excellent storage and sealing properties so that only a slight increment in releasing amount can be detected; a similar release condition can be found even with the increase of pH value to 7. By contrast, by increasing the pH value over pK_a (i.e., basic environment with pH > 7.4) and/or increasing the temperature above the LCST, the PDMAEMA brushes can be condensed to open the porous channels so that the loaded molecules can easily release and then diffuse into the release medium. Consequently, the delivery system with much higher release rate and sustained-release advantage can be observed at pH 8.5 and 25 °C. Similar release condition can be obtained at pH 7 and 65 °C.

In order to provide the elution profile associated with the PDMAEMA-functionalized nanoporous gyroid SiO_2, the release profiles were fitted by a semiempirical power law.[73,74]

$$M_t/M_{inf} = kt^n \quad (1)$$

where M_t standing the cumulative amount of released riboflavin at time t, M_{inf} standing the cumulative amount of released riboflavin at infinite time, t is time, k is the characteristic constant of the system, and n is the release exponent utilized to characterized the release mechanism. Using the first 60% of the fractional release curve, the fitted functions for part of the riboflavin-release profiles at pH 8.5 and 25 °C and at pH 7 and 65 °C can be acquired as shown in the insets a and b of Figure 7, respectively. As a result, the release profile is quite similar to Korsmeyer–Peppas equation with n = 1.23 and R^2 = 0.998 for the release environment at pH 8.5 and 25 °C and n = 1.35 and R^2 = 0.978 for the release environment at pH 7 and 65 °C, reflecting that the release mechanisms of loaded riboflavin from PDMAEMA-functionalized nanoporous gyroid SiO_2 is a super case II transport (occasionally, values of n > 0.89), and the release rate is a time-dependent process (rate as a function of time: t^{n-1}).[73,74] This release mechanism can result from the condensation of the grafted PDMAEMA brushes at the channel wall and therefore exhibit sustained-release property without burst release.

CONCLUSIONS

In summary, we create an environment-selective delivery system with efficient porous texture using nanoporous gyroid SiO_2 functionalized by double-stimuli-responsive PDMAEMA

dx.doi.org/10.1021/ma500360a | Macromolecules 2014, 47, 3041–3051

brushes, forming a biomimetic smart nanomaterial with high potential for versatile applications. Also, the temperature-resolved SAXS experiments were carried out for the first time to study the responsive properties of the grafted PDMAEMA brushes on the inner wall of the nanoporous gyroid SiO_2. The variations on the SAXS profiles give clear evidence for the conformational changes of PDMAEMA driven by varying the pH and temperature. According to the results of SAXS experiments, the double responsive properties can be successfully traced by altering the environment. Different releasing behavior can be observed in the cumulative release profiles of riboflavin-loaded PDMAEMA-functionalized nanoporous gyroid SiO_2 in response to different environments. The variations in the release behavior are mainly attributed to the double-stimuli-responsive properties of the grafted PDMAEMA brushes. When the environmental pH is below the pK_a and/or the temperature is below LCST, the fully protonated and extended PDMAEMA brushes can act as multiblockades that give excellent storage and sealing properties (i.e., at pH 1.5 and 25 °C). On the contrary, by increasing the pH value over pK_a and/or increasing the temperature above the LCST, the PDMAEMA brushes can be condensed to open the porous channels, giving a delivery system with much higher release rate and sustained-release advantage. Because of the environment-selective release behavior, the as-designed system can give double-stimuli-responsive controlled release (i.e., at pH 8.5 and 25 °C); for example, it can be designed as intestine targeted drug delivery that can avoid drug loss during the digestion and therefore improve the dose efficiency. Moreover, the PDMAEMA-functionalized nanoporous gyroid SiO_2 with well-defined structure, efficient porous texture, environmental resistance, and biocompatibility as well as double environmental stimuli gives the potential for being a versatile nanoreactor, such as nanoscale filter, environmental sensor, and biomimetic on/off gate.

■ ASSOCIATED CONTENT

Supporting Information

Figures S1–S6. This material is available free of charge via the Internet at http://pubs.acs.org.

■ AUTHOR INFORMATION

Corresponding Author

*Tel 886-3-5738349; Fax 886-3-5715408; e-mail rmho@mx.nthu.edu.tw (R.-M.H.).

Notes

The authors declare no competing financial interest.

■ ACKNOWLEDGMENTS

The authors acknowledge the financial support from the National Science Council of the Republic of China, Taiwan, under Contract NSC 102-2120-M-007-002 and Grant NSC 102-2633-M-007-002 as well as the National Synchrotron Radiation Research Center (NSRRC) for the assistance in the Synchrotron SAXS experiments. Last but not least, all the laboratory membranes and co-workers are appreciated for the kindly discussion and assistance.

■ REFERENCES

(1) de Las Heras Alarcon, C.; Pennadam, S.; Alexander, C. Stimuli Responsive Polymers for Biomedical Applications. *Chem. Soc. Rev.* **2005**, *34*, 276–285.

(2) Stuart, M. A. C.; Huck, W. T. S.; Genzer, J.; Müller, M.; Ober, C.; Stamm, M.; Sukhorukov, G. B.; Szleifer, I.; Tsukruk, V. V.; Urban, M.; Winnik, F.; Zauscher, S.; Luzinov, I.; Minko, S. Emerging Applications of Stimuli-Responsive Polymer Materials. *Nat. Mater.* **2010**, *9*, 101–113.

(3) Hoffmann, F.; Cornelius, M.; Morell, J.; Fröba, M. Silica-Based Mesoporous Organic-Inorganic Hybrid Materials. *Angew. Chem., Int. Ed.* **2006**, *45*, 3216–3251.

(4) Hou, X.; Guo, W.; Jiang, L. Biomimetic Smart Nanopores and Nanochannels. *Chem. Soc. Rev.* **2011**, *40*, 2385–2401.

(5) Wu, D.; Xu, F.; Sun, B.; Fu, R.; He, H.; Matyjaszewski, K. Design and Preparation of Porous Polymers. *Chem. Rev.* **2012**, *112*, 3959–4015.

(6) Furneaux, R. C.; Rigby, W. R.; Davidson, A. P. The Formation of Controlled-Porosity Membranes from Anodically Oxidized Aluminium. *Nature* **1989**, *337*, 147–149.

(7) Monnier, A.; Schuth, F.; Huo, Q.; Kumar, D.; Margolese, D.; Maxwell, R. S.; Stucky, G. D.; Krishnamurty, M.; Petroff, P.; Firouzi, A.; Janicke, M.; Chmelka, B. F. Cooperative Formation of Inorganic-Organic Interfaces in the Synthesis of Silicate Mesostructures. *Science* **1993**, *261*, 1299–1303.

(8) Schumacher, K.; Ravikovitch, P. I.; Chesne, A. D.; Neimark, A. V.; Unger, K. K. Characterization of MCM-48 Materials. *Langmuir* **2000**, *16*, 4648–4654.

(9) Bates, F. S.; Fredrickson, G. H. Block Copolymer Thermodynamics: Theory and Experiment. *Annu. Rev. Phys. Chem.* **1990**, *41*, 525–557.

(10) Bates, F. S.; Fredrickson, G. H. Block Copolymers - Designer Soft Materials. *Phys. Today* **1999**, *52*, 32–38.

(11) (a) Bockstaller, M. R.; Mickiewicz, R. A.; Thomas, E. L. Block Copolymer Nanocomposites: Perspectives for Tailored Functional Materials. *Adv. Mater.* **2005**, *17*, 1331–1349. (b) Jackson, E. A.; Hillmyer, M. A. Nanoporous Membranes Derived from Block Copolymers: from Drug Delivery to Water Filtration. *ACS Nano* **2010**, *4*, 3548–3553. (c) Schacher, F. H.; Rupar, P. A.; Manners, I. Functional Block Copolymers: Nanostructured Materials with Emerging Applications. *Angew. Chem., Int. Ed.* **2012**, *51*, 7898–7921. (d) Sinturel, C.; Vayer, M.; Morris, M.; Hillmyer, M. A. Solvent Vapor Annealing of Block Polymer Thin Films. *Macromolecules* **2013**, *46*, 5399–5415.

(12) Park, M.; Harrison, C.; Chaikin, P. M.; Register, R. A.; Adamson, D. H. Block Copolymer Lithography: Periodic Arrays of $\sim 10^{11}$ Holes in 1 Square Centimeter. *Science* **1997**, *276*, 1401–1404.

(13) Thurn-Albrecht, T.; Steiner, R.; DeRouchey, J.; Stafford, C. M.; Huang, E.; Bal, M.; Tuominen, M.; Hawker, C. J.; Russell, T. P. Nanoscopic Templates from Oriented Block Copolymer Films. *Adv. Mater.* **2000**, *12*, 787–791.

(14) Cheng, J. Y.; Ross, C. A.; Thomas, E. L.; Smith, H. I.; Vancso, G. J. Fabrication of Nanostructures with Long-Range Order Using Block Copolymer Lithography. *Appl. Phys. Lett.* **2002**, *81*, 3657–3659.

(15) Zalusky, A. S.; Olayo-Valles, R.; Taylor, C. J.; Hillmyer, M. A. Mesoporous Polystyrene Monoliths. *J. Am. Chem. Soc.* **2001**, *123*, 1519–1520.

(16) Hashimoto, T.; Tsutsumi, K.; Funaki, Y. Nanoprocessing Based on Bicontinuous Microdomains of Block Copolymers: Nanochannels Coated with Metals. *Langmuir* **1997**, *13*, 6869–6872.

(17) Chan, V. Z. H.; Hoffman, J.; Lee, V. Y.; Latrou, H.; Avgeropoulos, A.; Hadjichristidis, N.; Miller, R. D.; Thomas, E. L. Ordered Bicontinuous Nanoporous and Nanorelief Ceramic Films from Self Assembling Polymer Precursors. *Science* **1999**, *286*, 1716–1719.

(18) Cheng, J. Y.; Ross, C. A.; Chan, V. Z. H.; Thomas, E. L.; Lammertink, R. G. H.; Vancso, G. J. Formation of a Cobalt Magnetic Dot Array via Block Copolymer Lithography. *Adv. Mater.* **2001**, *13*, 1174–1178.

(19) (a) Tseng, W. H.; Chen, C. K.; Chiang, Y. W.; Ho, R. M.; Akasaka, S.; Hasegawa, H. Helical Nanocomposites from Chiral Block Copolymer Templates. *J. Am. Chem. Soc.* **2009**, *131*, 1356–1357. (b) Tseng, Y. T.; Tseng, W. H.; Lin, C. H.; Ho, R. M. Fabrication of

Double-Length-Scale Patterns via Lithography, Block Copolymer Templating, and Electrodeposition. *Adv. Mater.* **2007**, *19*, 3584−3588.
(20) Hajduk, D. A.; Harper, P. E.; Gruner, S. M.; Honeker, C. C.; Kim, G.; Thomas, E. L.; Fetters, L. J. The Gyroid: A New Equilibrium Morphology in Weakly Segregated Diblock Copolymers. *Macromolecules* **1994**, *27*, 4063−4075.
(21) Schulz, M. F.; Bates, F. S.; Almdal, K.; Mortensen, K. Epitaxial Relationship for Hexagonal-to-Cubic Phase Transition in a Book Copolymer Mixture. *Phys. Rev. Lett.* **1994**, *73*, 86−89.
(22) Matsen, M. W.; Schick, M. Stable and Unstable Phases of A Diblock Copolymer Melt. *Phys. Rev. Lett.* **1994**, *72*, 2660−2663.
(23) Detsi, E.; De Jong, E.; Zinchenko, A.; Vuković, Z.; Vukovic, I.; Punzhin, S.; Loos, K.; Brinke, G.; ten De Raedt, H. A.; Onck, P. R.; De Hosson, J. T. M. On The Specific Surface Area of Nanoporous Materials. *Acta Mater.* **2011**, *59*, 7488−7497.
(24) Li, L.; Schulte, L.; Clausen, L. D.; Hansen, K. M.; Jonsson, G. E.; Ndoni, S. Gyroid Nanoporous Membranes with Tunable Permeability. *ACS Nano* **2011**, *5*, 7754−7766.
(25) Crossland, E. J. W.; Kamperman, M.; Nedelcu, M.; Ducati, C.; Wiesner, U.; Smilgies, D. M.; Toombes, G. E. S.; Hillmyer, M. A.; Ludwigs, S.; Steiner, U.; Snaith, H. J. A Bicontinuous Double Gyroid Hybrid Solar Cell. *Nano Lett.* **2009**, *9*, 2807−2812.
(26) Finnemore, A. S.; Scherer, M. R. J.; Langford, R.; Mahajan, S.; Ludwigs, S.; Meldrum, F. C.; Steiner, U. Nanostructured Calcite Single Crystals with Gyroid Morphologies. *Adv. Mater.* **2009**, *21*, 3928−3932.
(27) Scherer, M. R. J.; Li, L.; Cunha, P. M. S.; Scherman, O. A.; Steiner, U. Enhanced Electrochromism in Gyroid-Structured Vanadium Pentoxide. *Adv. Mater.* **2012**, *24*, 1217−1221.
(28) Hsueh, H. Y.; Ho, R. M. Bicontinuous Ceramics with High Surface Area from Block Copolymer Templates. *Langmuir* **2012**, *28*, 8518−8529.
(29) Kim, E.; Vaynzof, Y.; Sepe, A.; Guldin, S.; Scherer, M.; Cunha, P.; Roth, S. V.; Scherer, M. R. J.; Steiner, U. Efficient Electrochromic Devices Made from 3D Nanotubular Gyroid Networks. *Nano Lett.* **2013**, *13*, 3005−3010.
(30) Steiner, U. Gyroid-Structured 3D ZnO Networks Made by Atomic Layer Deposition. *Adv. Funct. Mater.* **2014**, *24*, 863−872.
(31) Zarka, M. T.; Nuyken, O.; Weberskirch, R. Amphiphilic Polymer Supports for the Asymmetric Hydrogenation of Amino Acid Precursors in Water. *Chem.—Eur. J.* **2003**, *9*, 3228−3234.
(32) Rodionov, V.; Gao, H.; Scroggins, S.; Unruh, D. A.; Avestro, A. J.; Fréchet, J. M. J. Easy Access to a Family of Polymer Catalysts from Modular Star Polymers. *J. Am. Chem. Soc.* **2010**, *132*, 2570−2572.
(33) Choi, H. J.; Montemagno, C. D. Artificial Organelle: ATP Synthesis from Cellular Mimetic Polymersomes. *Nano Lett.* **2005**, *5*, 2538−2542.
(34) Vriezema, D. M.; Hoogboom, J.; Velonia, K.; Takazawa, K.; Christianen, P. C. M.; Maan, J. C.; Rowan, A. E.; Nolte, R. J. M. Vesicles and Polymerized Vesicles from Thiophene-Containing Rod−Coil Block Copolymers. *Angew. Chem.* **2003**, *115*, 796−800; *Angew. Chem., Int. Ed.* **2003**, *42*, 772−776.
(35) Broz, P.; Driamov, S.; Ziegler, J.; Ben-Haim, N.; Marsch, S.; Meier, W.; Hunziker, P. Toward Intelligent Nanosize Bioreactors: A pH-Switchable, Channel-Equipped, Functional Polymer Nanocontainer. *Nano Lett.* **2006**, *6*, 2349−2353.
(36) Lee, S. B.; Mitchell, D. T.; Trofin, L.; Nevanen, T. K.; Soderlund, H.; Martin, C. R. Antibody-Based Bio-Nanotube Membranes for Enantiomeric Drug Separations. *Science* **2002**, *296*, 2198−2200.
(37) Savariar, E. N.; Krishnamoorthy, K.; Thayumanavan, S. Molecular Discrimination Inside Polymer Nanotubules. *Nat. Nanotechnol.* **2008**, *3*, 112−117.
(38) Qiu, X.; Yu, H.; Karunakaran, M.; Pradeep, N.; Nunes, S. P.; Peinemann, K. V. Similarly Sized Proteins with Tunable Nanoporous Block Copolymer Membranes. *ACS Nano* **2013**, *7*, 768−776.
(39) Sparreboom, W.; van den Berg, A.; Eijkel, J. C. T. Principles and Applications of Nanofluidic Transport. *Nat. Nanotechnol.* **2009**, *4*, 713−720.
(40) Uehara, H.; Kakiage, M.; Sekiya, M.; Sakuma, D.; Yamonobe, T.; Takano, N.; Barraud, A.; Meurville, E.; Ryser, P. Size-Selective Diffusion in Nanoporous but Flexible Membranes for Glucose Sensors. *ACS Nano* **2009**, *3*, 924−932.
(41) Jiang, Y.; Liu, N.; Guo, W.; Xia, F.; Jiang, L. Highly-Efficient Gating of Solid-State Nanochannels by DNA Supersandwich Structure Containing ATP Aptamers: A Nanofluidic IMPLICATION Logic Device. *J. Am. Chem. Soc.* **2012**, *134*, 15395−15401.
(42) Zhou, Y.; Guo, W.; Cheng, J.; Liu, Y.; Li, J.; Jiang, L. High-Temperature Gating of Solid-State Nanopores with Thermo-Responsive Macromolecular Nanoactuators in Ionic Liquids. *Adv. Mater.* **2012**, *24*, 962−967.
(43) Liu, Z.; Luo, F.; Ju, X. J.; Xie, R.; Luo, T.; Sun, Y. M.; Chu, L. Y. Positively K^+-Responsive Membranes with Functional Gates Driven by Host−Guest Molecular Recognition. *Adv. Funct. Mater.* **2012**, *22*, 4742−4750.
(44) Clodt, J. I.; Filiz, V.; Rangou, S.; Buhr, K.; Abetz, C.; Höche, D.; Hahn, J.; Jung, A.; Abetz, V. Double Stimuli-Responsive Isoporous Membranes via Post-Modification of pH-Sensitive Self-Assembled Diblock Copolymer Membranes. *Adv. Funct. Mater.* **2013**, *23*, 731−738.
(45) Zhu, Y.; Shi, J.; Shen, W.; Dong, X.; Feng, J.; Ruan, M.; Li, Y. Stimuli-Responsive Controlled Drug Release from a Hollow Mesoporous Silica Sphere/Polyelectrolyte Multilayer Core−Shell Structure. *Angew. Chem., Int. Ed.* **2005**, *44*, 5083−5087.
(46) Slowing, I. I.; Vivero-Escoto, J. L.; Wu, C. W.; Lin, V. S. Mesoporous Silica Nanoparticles as Controlled Release Drug Delivery and Gene Transfection Carriers. *Adv. Drug Delivery Rev.* **2008**, *60*, 1278−1288.
(47) Lvov, Y. M.; Shchukin, D. G.; Möhwald, H.; Price, R. R. Halloysite Clay Nanotubes for Controlled Release of Protective Agents. *ACS Nano* **2008**, *2*, 814−820.
(48) Yah, W. O.; Takahara, A.; Lvov, Y. M. Selective Modification of Halloysite Lumen with Octadecylphosphonic Acid: New Inorganic Tubular Micelle. *J. Am. Chem. Soc.* **2012**, *134*, 1853−1859.
(49) Yah, W. O.; Xu, H.; Soejima, H.; Ma, W.; Lvov, Y.; Takahara, A. Biomimetic Dopamine Derivative for Selective Polymer Modification of Halloysite Nanotube Lumen. *J. Am. Chem. Soc.* **2012**, *134*, 12134−12137.
(50) Tang, F.; Li, L.; Chen, D. Mesoporous Silica Nanoparticles: Synthesis, Biocompatibility and Drug Delivery. *Adv. Mater.* **2012**, *24*, 1504−1534.
(51) Jeon, G.; Yang, S. Y.; Kim, J. K. Functional Nanoporous Membranes for Drug Delivery. *J. Mater. Chem.* **2012**, *22*, 14814−14834.
(52) Zhang, X.; Yang, P.; Dai, Y.; Ma, P.; Li, X.; Cheng, Z.; Hou, Z.; Kang, X.; Li, C.; Lin, J. Multifunctional Up-Converting Nanocomposites with Smart Polymer Brushes Gated Mesopores for Cell Imaging and Thermo/pH Dual-Responsive Drug Controlled Release. *Adv. Funct. Mater.* **2013**, *23*, 4067−4078.
(53) Mal, N. K.; Fujiwara, M.; Tanaka, Y. Photocontrolled Reversible Release of Guest Molecules from Coumarin-Modified Mesoporous Silica. *Nature* **2003**, *421*, 350−353.
(54) Nguyen, T. D.; Tseng, H. R.; Celestre, P. C.; Flood, A. H.; Liu, Y.; Stoddart, J. F.; Zink, J. I. A Reversible Molecular Valve. *Proc. Natl. Acad. Sci. U. S. A.* **2005**, *102*, 10029−10034.
(55) You, Y. Z.; Kalebaila, K. K.; Brock, S. L.; Oupický, D. Temperature Controlled Uptake and Release in PNIPAM-modified Mesoporous Silica Nanoparticles. *Chem. Mater.* **2008**, *20*, 3354−3359.
(56) Dai, S.; Ravi, P.; Tam, K. C. pH-Responsive Polymers: Synthesis, Properties and Applications. *Soft Matter* **2008**, *4*, 435−449.
(57) Meng, F.; Zhong, Z.; Feijen, J. Stimuli-Responsive Polymersomes for Programmed Drug Delivery. *Biomacromolecules* **2009**, *10*, 197−209.
(58) Synatschke, C. V.; Schallon, A.; Jerome, V.; Freitag, R.; Müller, A. H. E. Influence of Polymer Architecture and Molecular Weight of Poly(2-(dimethylamino)ethyl methacrylate) Polycations on Transfection Efficiency and Cell Viability in Gene Delivery. *Biomacromolecules* **2011**, *12*, 4247−4255.

(59) Georgiou, T. K.; Vamvakaki, M.; Patrickios, C. S.; Yamasaki, E. N.; Phylactou, L. A. Nanoscopic Cationic Methacrylate Star Homopolymers: Synthesis by Group Transfer Polymerization, Characterization and Evaluation as Transfection Reagents. *Biomacromolecules* **2004**, *5*, 2221−2229.
(60) Xu, F. J.; Ping, Y.; Ma, J.; Tang, G. P.; Yang, W. T.; Li, J.; Kang, E. T.; Neoh, K. G. Comb-Shaped Copolymers Composed of Hydroxypropyl Cellulose Backbones and Cationic Poly((2-dimethyl amino)ethyl methacrylate) Side Chains for Gene Delivery. *Bioconjugate Chem.* **2009**, *20*, 1449−1458.
(61) Schacher, F.; Ulbricht, M.; Müller, A. H. E. Self-Supporting, Double Stimuli-Responsive Porous Membranes From Polystyrene-Block-Poly(N,N-dimethylaminoethyl methacrylate) Diblock Copolymers. *Adv. Funct. Mater.* **2009**, *19*, 1040−1045.
(62) van de Wetering, P.; Zuidam, N. J.; van Steenbergen, M. J.; van der Houwen, O. A. G. J.; Underberg, W. J. M.; Hennink, W. E. A Mechanistic Study of the Hydrolytic Stability of Poly(2-(dimethylamino)ethyl methacrylate). *Macromolecules* **1998**, *31*, 8063−8068.
(63) Plamper, F.; Ruppel, M.; Schmalz, A.; Borisov, O.; Ballauff, M.; Müller, A. H. E. Tuning the Thermoresponsive Properties of Weak Polyelectrolytes: Aqueous Solutions of Star-Shaped and Linear Poly(N,N-dimethylaminoethyl Methacrylate). *Macromolecules* **2007**, *40*, 8361−8366.
(64) Fournier, D.; Hoogenboom, R.; Thijs, H. M. L.; Paulus, R. M.; Schubert, U. S. Tunable pH- and Temperature-Sensitive Copolymer Libraries by Reversible Addition−Fragmentation Chain Transfer Copolymerizations of Methacrylates. *Macromolecules* **2007**, *40*, 915−920.
(65) Ho, R. M.; Chiang, Y. W.; Chen, C. K.; Wang, H. W.; Hasegawa, H.; Akasaka, S.; Thomas, E. L.; Burger, C.; Hsiao, B. S. Block Copolymers with A Twist. *J. Am. Chem. Soc.* **2009**, *131*, 18533−18542.
(66) Hsueh, H. Y.; Chen, H. Y.; She, M. S.; Chen, C. K.; Ho, R. M.; Gwo, S.; Hasegawa, H.; Thomas, E. L. Inorganic Gyroid with Exceptionally Low Refractive Index from Block Copolymer Templating. *Nano Lett.* **2010**, *10*, 4994−5000.
(67) Sakata, H.; Kobayashi, M.; Otsuka, H.; Takahara, A. Tribological Properties of Poly(methyl methacrylate) Brushes Prepared by Surface-Initiated Atom Transfer Radical Polymerization. *Polym. J.* **2005**, *37*, 767−775.
(68) Zhang, X.; Xia, J. H.; Matyjaszewski, K. Controlled/"Living" Radical Polymerization of 2-(Dimethylamino)ethyl Methacrylate. *Macromolecules* **1998**, *31*, 5167−5169.
(69) Dair, B. J.; Honeker, C. C.; Alward, D. B.; Avgeropoulos, A.; Hadjichristidis, N.; Fetters, L. J.; Capel, M.; Thomas, E. L. Mechanical Properties and Deformation Behavior of the Double Gyroid Phase in Unoriented Thermoplastic Elastomers. *Macromolecules* **1999**, *32*, 8145−8152.
(70) Sakurai, S.; Isobe, D.; Okamoto, S.; Yao, T.; Nomural, S. Collapse of the Ia3̄d Cubic Symmetry by Uniaxial Stretching of A Double-Gyroid Block Copolymer. *Phys. Rev. E* **2001**, *63*, 061803.
(71) Saranathan, V.; Osuji, C. O.; Mochrie, S. G. J.; Noh, H.; Narayanan, S.; Sandy, A.; Dufresne, E. R.; Prum, R. O. Structure, Function, and Self-Assembly of Single Network Gyroid (I4132) Photonic Crystals in Butterfly Wing Scales. *Proc. Natl. Acad. Sci. U. S. A.* **2010**, *107*, 11676−11681.
(72) Hsueh, H. Y.; Ling, Y. C.; Wang, H. F.; Chang Chien, L. Y.; Hung, Y. C.; Thomas, E. L.; Ho, R. M. Shifting Networks to Achieve Subgroup Symmetry Properties. *Adv. Mater.* **2014**, DOI: 10.1002/adma.201305618.
(73) Korsemeyer, R. W.; Gurny, R.; Doelker, E.; Buri, P.; Peppas, N. A. Mechanism of Solute Release from Porous Hydrophilic Polymers. *Int. J. Pharm.* **1983**, *15*, 25−35.
(74) Dash, S.; Murthy, P. N.; Nath, L.; Chowdhury, P. Kinetic Modeling on Drug Release from Controlled Drug Delivery Systems. *Acta Polym. Pharm.* **2010**, *67*, 217−223.
(75) Warren, S. C.; Messina, L. C.; Slaughter, L. S.; Kamperman, M.; Zhou, Q.; Gruner, S. M.; DiSalvo, F. J.; Wiesner, U. Ordered Mesoporous Materials from Metal Nanoparticle−Block Copolymer Self-Assembly. *Science* **2008**, *320*, 1748−1752.